ADVANCED MATERIALS INTERFACES
www.advmatinterfaces.de

Direct Atomic Layer Deposition of Ultrathin Aluminum Oxide on Monolayer MoS_2 Exfoliated on Gold: The Role of the Substrate

Emanuela Schilirò, Raffaella Lo Nigro, Salvatore E. Panasci, Simonpietro Agnello, Marco Cannas, Franco M. Gelardi, Fabrizio Roccaforte, and Filippo Giannazzo**

In this paper, the authors demonstrate the atomic layer deposition (ALD) of highly homogeneous and ultrathin (≈3.6 nm) Al_2O_3 films with very good insulating properties (breakdown field of ≈10–12 MV cm^{-1}) directly onto monolayer (1L) MoS_2 exfoliated on gold. Differently than in the case of 1L MoS_2 supported by a common insulating substrate (Al_2O_3/Si), a better nucleation process of the high-*k* film is observed on the 1L MoS_2/Au system since the ALD early stages. Atomic force microscopy analyses show a ≈50% Al_2O_3 surface coverage just after 10 ALD cycles, its increase to >90% (after 40 cycles), and a uniform ≈3.6 nm film (after 80 cycles). The Al_2O_3 density on bilayer MoS_2 is found to be significantly reduced with respect to 1L MoS_2/Au, suggesting a role of screened interface charges with the metal substrate on the adsorption of ALD precursors. Finally, Raman and photoluminescence spectroscopy show a p-type doping and tensile strain of 1L MoS_2 induced by the Au substrate, providing an insight on the evolution of vibrational and optical properties after the Al_2O_3 deposition. The direct ALD growth of Al_2O_3 on large-area 1L MoS_2 induced by the Au underlayer can be of wide interest for electronic applications.

1. Introduction

Semiconducting transition metal dichalcogenides (TMDs), including MoS_2, WS_2, $MoSe_2$, and WSe_2, are currently widely investigated for next generation electronic and optoelectronic applications.[1,2] The deposition of high-*k* dielectrics thin films (such as Al_2O_3 and HfO_2) on the TMDs surface represents a key requirement for the fabrication of electronic devices.[3–5] As an example, the deposition of a HfO_2 gate insulator (≈30 nm thick) on top of monolayer (1L) MoS_2 represented the enabling step to demonstrate a field-effect transistor (FET) with excellent on/off ratio (≈10^8), nearly ideal subthreshold swing (≈70 mV dec^{-1}), and high room temperature electron mobility (>200 cm^2 V^{-1} s^{-1}), due to the efficient reduction of charged impurities scattering because of the high-*k* dielectric film.[6] Similarly, an Al_2O_3 top gate dielectric (≈16 nm thick) was employed for the demonstration of a high mobility (≈125 cm^2 V^{-1} s^{-1}) multilayer MoS_2 transistor.[7] In all these cases, the high-*k* dielectric films were grown by the atomic layer deposition (ALD) technique,[8] commonly employed in microelectronics to obtain uniform and conformal insulating films with a subnanometric control of the thickness. Ideally, layer-by-layer deposition of ultrathin films requires the presence of a sufficiently high and uniform density of dangling bonds, necessary for precursor chemisorption on the sample surface in the early stages of the ALD process.[9,10] However, the inherent lack of out-of-plane bonds in 2D layered materials represents an obstacle for an ideal ALD growth, resulting in an inhomogeneous coverage especially for very thin (<10 nm) deposited films.[11,12] In this context, relatively thick high-*k* films were employed in the first pioneering studies on MoS_2 transistors to achieve a uniform coverage of MoS_2 surface, thus minimizing the gate leakage current. However, the real application of MoS_2 FETs in next generation logic devices requires an aggressive scaling of the channel length and, consequently, of the high-*k* dielectric thickness.[3] Hence, several strategies have been investigated in the last few years to improve the ALD growth on TMDs, by tailoring the process conditions and/or by appropriate prefunctionalization treatments of the surface. Many of these approaches were inspired by ALD growth

E. Schilirò, R. L. Nigro, S. E. Panasci, S. Agnello, F. Roccaforte, F. Giannazzo
CNR-IMM
Strada VIII, 5, Catania 95121, Italy
E-mail: raffaella.lonigro@imm.cnr.it; filippo.giannazzo@imm.cnr.it
S. E. Panasci
Department of Physics and Astronomy
University of Catania
Via Santa Sofia 64, Catania 95123, Italy
S. Agnello, M. Cannas, F. M. Gelardi
Department of Physics and Chemistry Emilio Segrè
University of Palermo
Via Archirafi 36, Palermo 90123, Italy
S. Agnello
ATeN Center
University of Palermo
Viale delle Scienze Ed. 18, Palermo 90128, Italy

The ORCID identification number(s) for the author(s) of this article can be found under https://doi.org/10.1002/admi.202101117.

© 2021 The Authors. Advanced Materials Interfaces published by Wiley-VCH GmbH. This is an open access article under the terms of the Creative Commons Attribution License, which permits use, distribution and reproduction in any medium, provided the original work is properly cited.

DOI: 10.1002/admi.202101117

experiments performed on graphene.[13–15] As an example, Park et al.[10] systematically investigated thermal ALD of Al_2O_3, using trimethyl-aluminum (TMA) as the Al precursor and water (H_2O) as coreactant, on the surface of different TMDs, that is, MoS_2, WS_2, and WSe_2 multilayers. The deposition temperature (T_{dep}) and the TMA adsorption energy (E_{ads}) on the TMDs surface were demonstrated to play a crucial role on the uniformity of the deposited Al_2O_3 (≈10 nm) films. In particular, E_{ads}, which is related to the substrate polarizability, was found to be larger for W- and Se-based TMDs (e.g., WS_2 and WSe_2) than for MoS_2. Furthermore, while inhomogeneous Al_2O_3 films (with a large density of pinholes) were obtained at typical T_{dep} from 200 to 250 °C, the coverage uniformity was highly improved by lowering T_{dep} to 150 °C, that is, reducing the desorption of the metal precursors from the MoS_2 surface.[10] A two-step ALD process,[16] consisting in the low temperature (80 °C) deposition of an ultrathin AlOx layer, followed by a second ALD step at higher temperature (180 °C), was also employed to obtain a homogeneous Al_2O_3 film with <10 nm total thickness on MoS_2.[17] Although the use of a reduced temperature at the beginning or during the whole ALD process can be beneficial to improve the coverage uniformity, it may result in a lower dielectric quality due to a reduced reactivity of the ALD-precursors.[18] Another strategy to improve the ALD growth on MoS_2 surface has been to replace H_2O with a more reactive coreactant, such as ozone (O_3), which allowed to obtain uniform Al_2O_3 layers (≈5 nm thick) at a temperature of 200 °C.[19] Alternatively, an O_2-plasma pretreatment of multilayer MoS_2 surface, resulting in the formation of an ultrathin Mo-oxide layer, was shown to significantly improve the uniformity of the deposited Al_2O_3 or HfO_2 films as compared to the case of pristine MoS_2.[20] More recently, water plasma pretreatments of the MoS_2 surface have been used to create hydroxyl groups for conventional thermal ALD at 200–250 °C, resulting in the deposition of uniform Al_2O_3 films with thickness down to 1.5 nm.[21] In spite of these beneficial effects, the damage and chemical modifications introduced by these plasma pretreatments can affect the electronic transport in MoS_2 devices. Besides thermal ALD, plasma-enhanced ALD (PEALD) processes have also been recently investigated to grow very thin films (<5 nm) of Al_2O_3 and HfO_2 on MoS_2 samples with different layer numbers.[22,23] In particular, electrical characterization of 1L, bilayer (2L), and trilayer MoS_2 back-gated transistors before and after HfO_2 PEALD revealed the occurrence of plasma damage, resulting in significant degradation of the electronic properties especially for 1L MoS_2.[23]

In addition to these processes involving a chemical modification of MoS_2 surface, non-covalent functionalization with thin organic (e.g., perylene derivatives)[24] or inorganic (e.g., SiO_2 nanoparticles)[25] seeding layers has also been explored to promote the thermal ALD growth of thin Al_2O_3 films on MoS_2. However, the use of these interlayers ultimately limits the minimum thickness of the dielectric and may affect the electrical quality of the interface.

This short overview about ALD of high-*k* dielectrics on TMDs indicates that the seeding layers and prefunctionalization approaches explored so far present some disadvantages, while direct thermal ALD of ultrathin films would be highly desirable. In this respect, the interaction of atomically thin MoS_2 layers with the underlying substrate is expected to play an important role in the ALD nucleation stage, similarly to what observed for 1L graphene residing on some specific substrates.[26,27] As an example, Dlubak et al.[26] reported an enhanced Al_2O_3 nucleation on CVD-grown 1L graphene residing on the native metal substrates (Cu, Ni), that was ascribed to an improved ALD-precursor adsorption due the electrostatic effect of polar traps located at graphene/metal interface.[28,29] More recently, the uniform growth of ultrathin (≈2.4 nm) Al_2O_3 films by direct thermal ALD (at 250 °C) on 1L epitaxial graphene on 4H-SiC(0001) has been ascribed to the beneficial effect of the carbon buffer layer at the interface with the substrate.[30] To the best of our knowledge, analogous substrate effects on the ALD nucleation onto 1L TMDs have not been reported so far.

In this paper, we investigated the ALD growth of ultrathin (3.6 nm) Al_2O_3 films on 1L MoS_2 produced by gold-assisted mechanical exfoliation from bulk crystals.[31–34] This method exploits the strong Au–S interaction to exfoliate large-area (cm^2) MoS_2 membranes, predominantly formed by monolayers, on a gold substrate. These high crystalline quality membranes can be subsequently transferred on insulating substrates.[33,34]

Using identical ALD conditions on 1L MoS_2 membranes supported by gold (MoS_2/Au) or by Al_2O_3(100 nm)/Si substrate (MoS_2/Al_2O_3/Si), the typical inhomogeneous coverage by Al_2O_3 islands was observed in the case of the 1L MoS_2/Al_2O_3/Si system, whereas the formation of a highly uniform Al_2O_3 film (≈3.6 nm thick) with very good insulating properties (breakdown field of 10–12 MV cm^{-1}) was observed on the 1L MoS_2/Au sample. This excellent uniformity is the result of an enhanced ALD nucleation on MoS_2 surface due to the interaction with Au substrate, giving rise to ≈50% Al_2O_3 surface coverage after only 10 ALD cycles, and >90% coverage after 40 cycles. Further analysis by micro-Raman and micro-photoluminescence (PL) spectroscopy provided an insight on the substrate-related doping and strain of MoS_2/Au and MoS_2/Al_2O_3 samples, as well as on the effect of the ALD process on the vibrational and optical emission properties.

2. Results and Discussion

Figure 1a,b shows two representative atomic force microscopy (AFM) images of the Au/Ni/SiO_2 and Al_2O_3/Si starting substrates. A smooth surface morphology is observed in both cases, with similar root mean square roughness (RMS) values of 0.18 and 0.23 nm, respectively. Figure 1c,d shows two AFM images collected after exfoliation and transfer of MoS_2 on the Au/Ni/SiO_2 and Al_2O_3/Si substrates, respectively. For both samples, a region where the MoS_2 membrane was partially covering the substrate is shown, and the ≈0.7 nm step height in the line profiles (insets of Figure 1c,d) confirms 1L MoS_2 thickness. Finally, two higher resolution morphological images of 1L MoS_2/Au and 1L MoS_2/Al_2O_3 are reported in Figures 1e and 1f, respectively, from which similar RMS values (0.17 and 0.18 nm) to those measured on the bare substrates were obtained.

Figure 2 shows the comparison between the AFM surface morphologies of Al_2O_3 simultaneously deposited at 250 °C by 80 ALD cycles on the surface of the 1L MoS_2/Al_2O_3/Si sample (a) and of the 1L MoS_2/Au sample (b), respectively. A high RMS roughness of 2.5 nm was observed for Al_2O_3 deposited on 1L MoS_2 supported by the Al_2O_3/Si substrate. This RMS value

© 2021 The Authors. Advanced Materials Interfaces published by Wiley-VCH GmbH

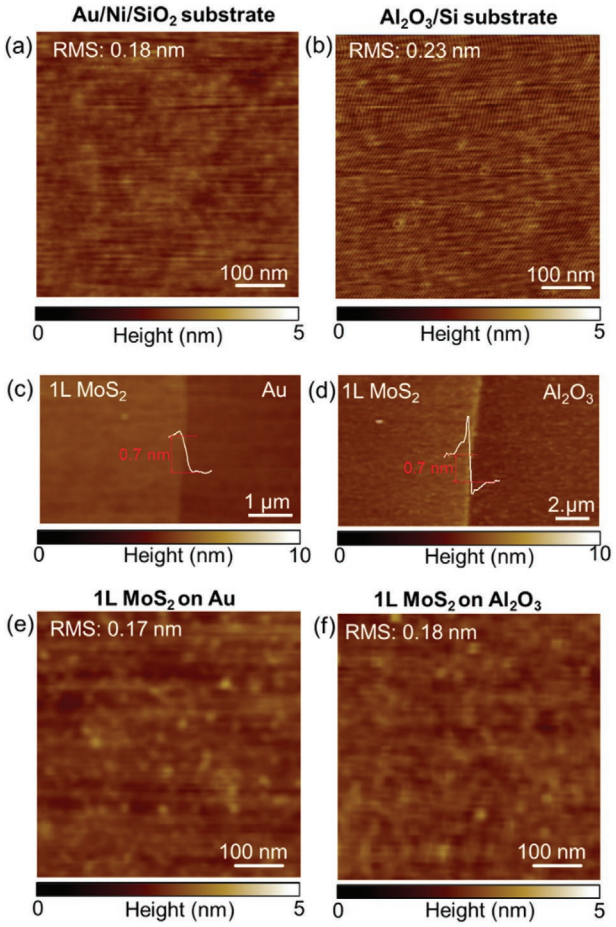

Figure 1. AFM morphologies of the a) Au/Ni/SiO_2 and b) Al_2O_3/Si substrates, with indicated the root mean square (RMS) roughness values. Low magnification AFM images of 1L MoS_2 partially covering the surface of c) Au and d) Al_2O_3. In both cases, the measured step height of ≈0.7 nm on the height line profiles confirms 1L MoS_2 thickness. AFM morphologies of the 1L MoS_2 on e) Au and on f) Al_2O_3 substrates; RMS roughness values are indicated.

is much larger than the ones of the original Al_2O_3 substrate (≈0.23 nm) and of 1L MoS_2 on Al_2O_3 (≈0.18 nm), indicating a very inhomogeneous coverage of 1L MoS_2 by the ALD grown Al_2O_3. This scenario, schematically depicted in Figure 2c, is consistent with the commonly reported island growth during direct thermal ALD on MoS_2 surface. In order to evaluate the Al_2O_3 coverage, the histogram of height distribution has been reported in Figure 2e. This histogram shows two components, related to bare and Al_2O_3-covered MoS_2 areas, from which ≈70% coverage and an average Al_2O_3 islands height of ≈4 nm were deduced. Differently, for 1L MoS_2 supported by the Au substrate (Figure 2b), a pinhole-free Al_2O_3 layer with a very flat morphology is observed after 80 ALD cycles. The deposited film exhibits a very narrow height distribution (Figure 2f) and low surface roughness (RMS = 0.25 nm), only slightly higher than the one measured on bare 1L MoS_2 on Au (RMS = 0.17 nm).[32] Such morphological results suggest that, under identical process conditions, an enhanced Al_2O_3 nucleation occurs on the surface of 1L MoS_2 in contact with gold, resulting in the formation of a continuous Al_2O_3 film, as schematically depicted in Figure 2d.

In order to evaluate the thickness and the electrical insulating quality of the uniform Al_2O_3 film deposited on 1L MoS_2/Au, conductive AFM (C-AFM) morphology and current maps were simultaneously acquired by scanning the metal tip across a step between the Al_2O_3/1L MoS_2 stack and the underlying Au substrate, as schematically depicted in **Figure 3**a. Figure 3b shows a morphological image collected in the proximity of a crack in the 1L MoS_2 membrane. The growth of a uniform and compact Al_2O_3 film on 1L MoS_2 and a poor ALD growth on the bare Au surface can be deduced from this image. Furthermore, the height line-profile in Figure 3c displays a total thickness of the Al_2O_3/MoS_2 stack of ≈4.3 nm, from which a deposited Al_2O_3 thickness of ≈3.6 nm can be estimated, by subtracting the thickness of 1L MoS_2 on Au (≈0.7 nm).[34] The slightly increased height observed at the step edge can be ascribed to the folding of the broken 1L MoS_2 membrane. The electrical insulating properties of the 3.6 nm Al_2O_3 film deposited onto 1L MoS_2 on Au are demonstrated by the current map in Figure 3d, acquired by applying a bias of 3 V between the tip and the gold substrate. In particular, the line-profile in Figure 3e shows very low current values in the Al_2O_3/1L MoS_2 region, whereas the saturation value of the current sensor was reached on Au region. The current conduction in the region close to the step edge suggests lower insulating properties of Al_2O_3 deposited on the locally folded MoS_2 membrane.

To get further insight on the electrical insulating quality of the 3.6 nm Al_2O_3 film, local current–voltage (I–V) characteristics were acquired by the C-AFM tip on the Al_2O_3/1L MoS_2/Au stack. **Figure 4**a shows three representative I–V curves measured at different positions on the Al_2O_3 surface by ramping the bias from 0 to 5 V. While very low leakage current values are observed up to ≈3 V, an abrupt rise of current up to the compliance level (indicating a localized dielectric breakdown) occurs at bias values in the range from 3.7 to 4.5 V, depending on the local I–V curve. For the Al_2O_3 film thickness t_{ox} = 3.6 nm, these breakdown voltage (V_{BD}) values correspond to breakdown electric fields ($E_{BD} = V_{BD}/t_{ox}$) of ≈10–12 MV cm^{-1}. These values are comparable to those reported for the state-of-the-art high-k dielectrics with similar equivalent oxide thickness deposited by ALD on MoS_2.[35] The localized nature of the breakdown events is further confirmed by the current map in Figure 4b, acquired on the surface of the Al_2O_3/1L MoS_2/Au stack while changing the bias from 3 V (in the upper part of the image) to 4 V (in the middle part) and then back to 3 V (bottom part). An increase of the leakage current level is observed when increasing the bias from 3 to 4 V, with the appearance of conduction instability and some localized breakdown spots. After reducing the bias down to 3 V (bottom part of the image), the current level becomes identical to the one in the upper part, confirming the localized character of the breakdown behavior.

After demonstrating the formation of a compact ≈3.6 nm Al_2O_3 insulating film on top of 1L MoS_2/Au by 80 ALD cycles at 250 °C, we investigated the film nucleation and growth stages by AFM analyses performed after a reduced number of ALD cycles at the same temperature.

Figure 5a,d shows the tapping mode morphological images acquired on 1L MoS_2/Au samples after 10 and 40 ALD cycles, respectively. The AFM analysis of the sample after 80 ALD cycles is also reported in Figure 5g for comparison. In

© 2021 The Authors. Advanced Materials Interfaces published by Wiley-VCH GmbH

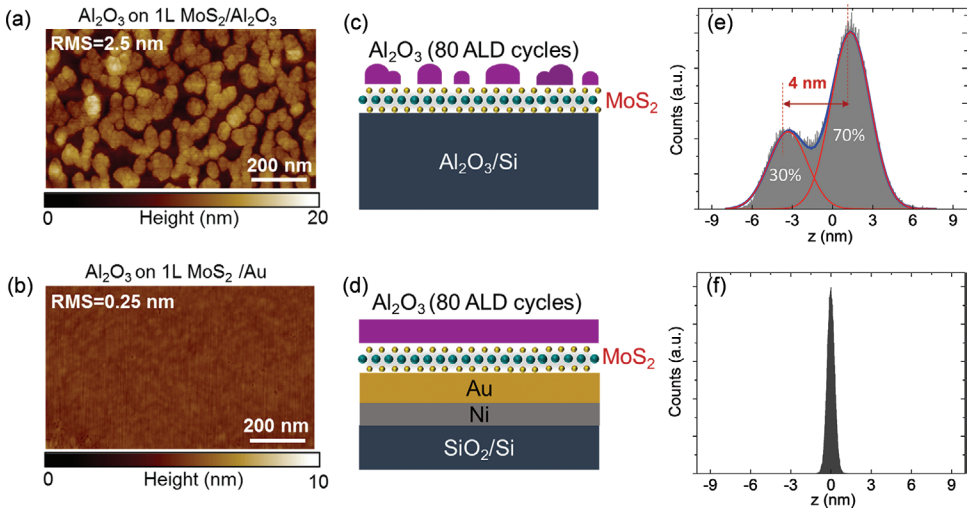

Figure 2. AFM morphologies of Al_2O_3 simultaneously deposited at 250 °C by 80 ALD cycles on the surface of the a) 1L $MoS_2/Al_2O_3/Si$ sample and of the b) 1L MoS_2/Au sample. The root mean square (RMS) roughness values of the two samples are indicated. c,d) Schematic illustrations of the configurations of the deposited Al_2O_3 on 1L $MoS_2/Al_2O_3/Si$ and 1L MoS_2/Au. e) Histogram of the height distribution obtained from the AFM map of Al_2O_3 on 1L $MoS_2/Al_2O_3/Si$, from which ≈70% Al_2O_3 coverage and an average height of ≈4 nm of Al_2O_3 islands were evaluated. f) Histogram of the height distribution for Al_2O_3 on 1L MoS_2/Au.

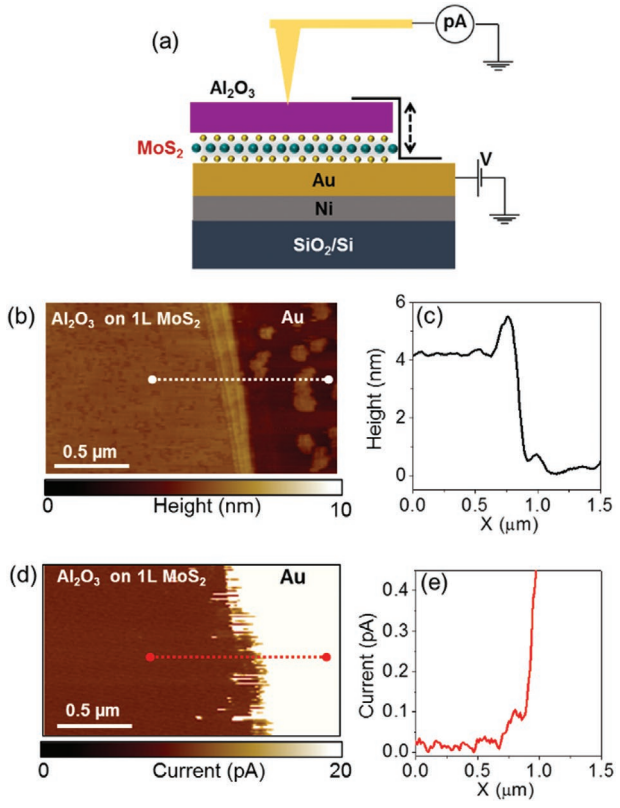

Figure 3. a) Schematic of the step between the Al_2O_3/1L MoS_2 stack and the underlying Au substrate and of the circuit used for C-AFM measurements. b) AFM image and c) height line-profile of the step, from which a deposited Al_2O_3 with thickness of ≈3.6 nm was estimated, after subtracting 1L MoS_2 thickness (≈0.7 nm). d) C-AFM current map simultaneously acquired with a bias $V = 3$V and e) current profile, demonstrating a good insulating quality of the deposited Al_2O_3 film onto 1L MoS_2 on Au.

particular, after ten cycles, a very irregular and ultrathin coating can be deduced from the morphological image, resulting in a RMS ≈ 0.4 nm, slightly higher than the ≈0.17 nm value measured on the bare 1L MoS_2/Au sample. On the other hand, a grain-shaped morphology (RMS ≈ 0.6 nm) of the deposited Al_2O_3 film can be clearly observed after 40 ALD cycles (see Figure 5d), suggesting the occurrence of 3D growth of Al_2O_3 islands on top of the inhomogeneous nucleation layer formed at lower number of cycles. Finally, a flat surface morphology (RMS ≈ 0.25 nm) is observed after 80 ALD cycles (Figure 5g). A quantification of the coverage percentage is very difficult from these morphological images. On the other hand, the Al_2O_3-coated and uncoated 1L MoS_2 areas can be clearly distinguished in the corresponding AFM phase maps (Figure 5b,e,h), as the phase signal is known to be very sensitive to the surface properties of materials. In particular, the red and black contrast in these three images corresponds to the Al_2O_3-covered and

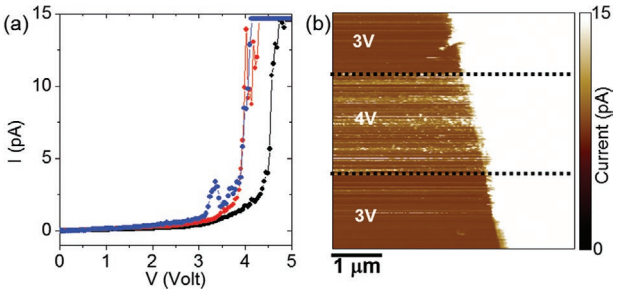

Figure 4. a) Local current–voltage (*I*–*V*) characteristics collected at different positions on the Al_2O_3/MoS_2/Au stack, showing current breakdown at biases between 3.7 and 4.5 V. b) C-AFM current map collected on the Al_2O_3/MoS_2/Au stack at bias values of 3 V (upper region), 4 V (middle region), and 3 V (bottom region). A significant increase of the current leakage, with the appearance of localized breakdown spots is observed at 4 V.

© 2021 The Authors. Advanced Materials Interfaces published by Wiley-VCH GmbH

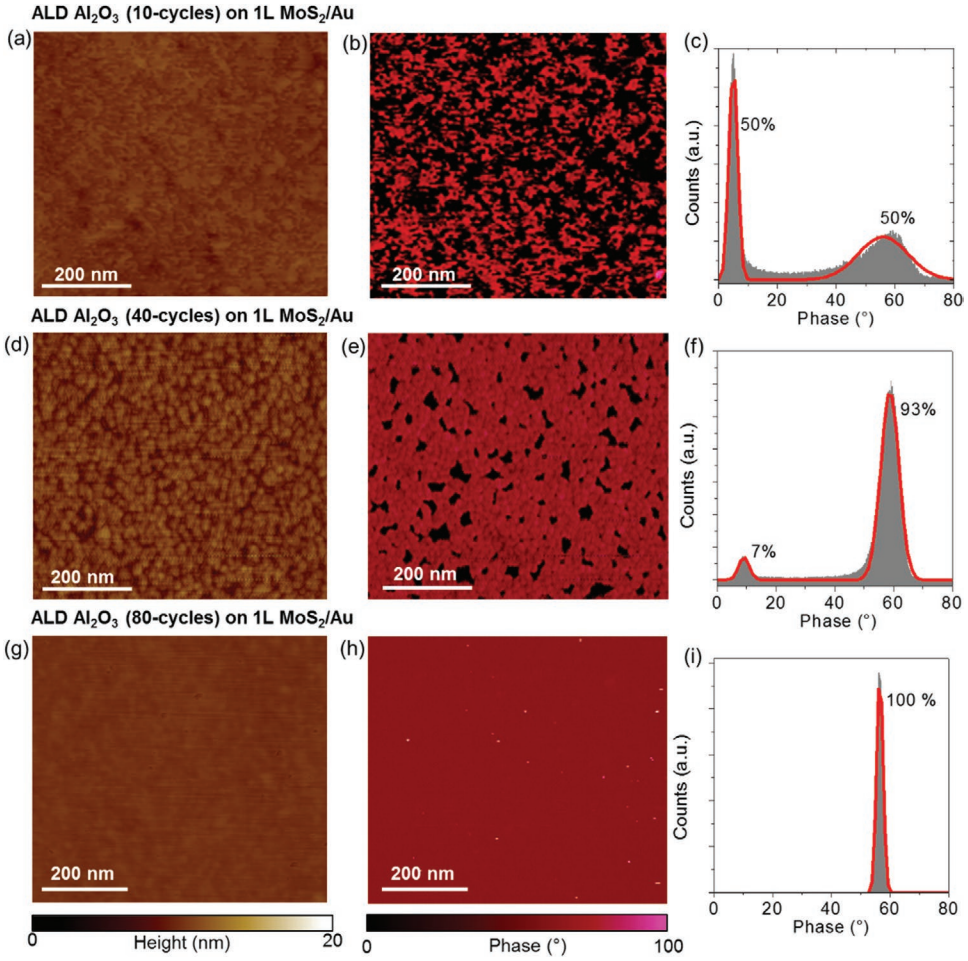

Figure 5. a) AFM morphology and b) phase map measured after 10 Al_2O_3 ALD cycles on 1L MoS_2/Au. c) Histogram of the phase distribution and evaluation of the Al_2O_3 coverage percentage on the same sample. d) AFM morphology and e) phase map measured after 40 Al_2O_3 ALD cycles on 1L MoS_2/Au. f) Histogram of the phase distribution and evaluation of the Al_2O_3 coverage percentage on the same sample. g) AFM morphology and h) phase map measured after 80 Al_2O_3 ALD cycles on 1L MoS_2/Au. i) Histogram of the phase distribution and evaluation of the Al_2O_3 coverage percentage on the same sample.

uncovered 1L MoS_2, respectively. Furthermore, the histograms of the phase distribution extracted from the three maps are reported in Figure 5c,f,i, from which an Al_2O_3 coverage percentage of 50%, 93%, and 100% were evaluated after 10, 40, and 80 ALD cycles, respectively. The very high coverage after only 40 ALD cycles, corresponding to ≈1.4 nm Al_2O_3 thickness (measured by an AFM step-height analysis as in Figure 3b), demonstrates a very good nucleation on Au supported 1L MoS_2.

Interestingly, the coverage degree of ALD grown Al_2O_3 was found to be strongly dependent on the number of MoS_2 layers. **Figure 6**a,b shows typical AFM morphology and phase maps measured on the as-exfoliated MoS_2/Au sample including 1L and 2L MoS_2 regions. The two regions exhibit similar surface roughness and the same uniform phase signal. Figure 6c,d shows the morphology (c) and phase images (d) collected in a 1L/2L area of the MoS_2/Au sample after 40 ALD cycles. A very different Al_2O_3 coverage can be clearly observed (especially in the phase image) on 1L and 2L MoS_2 regions, with a much denser Al_2O_3 nucleation on 1L than on the 2L MoS_2.

The above-illustrated experimental phenomena, that is, the enhanced Al_2O_3 nucleation on 1L MoS_2 supported by Au and its reduction on 2L regions, exhibit close similarities to reported ALD growth on CVD graphene on metals (Ni and Cu)[26] and on epitaxial graphene on 4H-SiC.[27] In the first case, the optimal Al_2O_3 nucleation on 1L graphene during thermal ALD with H_2O and TMA precursors was ascribed to the enhanced adsorption of the polar H_2O molecules due to the electrostatic field generated by charged dipoles located at graphene/metal interface.[26] In the case of epitaxial graphene on 4H-SiC, the electrostatic field due to charges at buffer layer/SiC interface was found to play a similar role.[27] In both cases, the intensity of this electrostatic field was drastically reduced in 2L graphene, due to the screening effect, resulting in a less homogeneous Al_2O_3 growth. A similar mechanism can be considered in the present case to explain the Al_2O_3 nucleation on 1L and 2L MoS_2 supported by Au. Furthermore, the significant tensile strain experienced by the 1L MoS_2 membrane exfoliated on Au can also play an important role, as discussed in the following.

© 2021 The Authors. Advanced Materials Interfaces published by Wiley-VCH GmbH

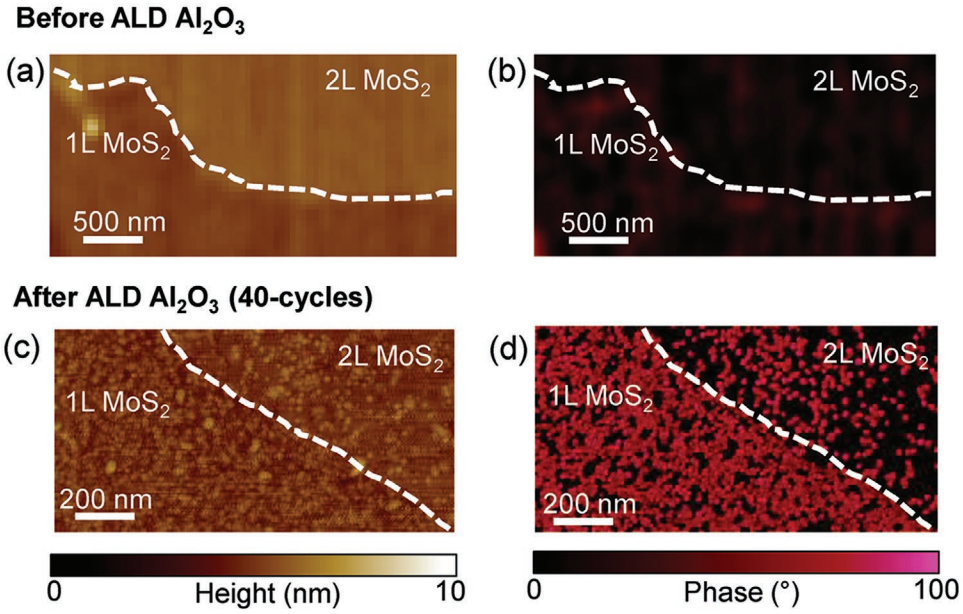

Figure 6. a) AFM-morphology and b) phase image of 1L and 2L MoS_2 on Au before the Al_2O_3 deposition by ALD. c) AFM-morphology and d) phase image of the Al_2O_3 deposited by 40 ALD cycles both on 1L and 2L MoS_2 on Au regions.

Micro-Raman spectroscopy analyses have been performed to investigate the strain and doping status of 1L MoS_2 residing on Au and Al_2O_3 substrates before and after the ALD growth. **Figure 7**a reports two representative Raman spectra for as-exfoliated 1L MoS_2 on Au (reference) and after 80 TMA/H_2O ALD cycles, resulting in the homogeneous ≈3.6 nm Al_2O_3 film deposition shown in Figure 3b. The corresponding Raman spectra for 1L MoS_2 transferred onto the Al_2O_3/Si substrate (reference) and after the 80 ALD cycles are shown in Figure 7b. From the comparison of the reference spectra on the two substrates, a significantly higher separation $\Delta\omega$ between the in-plane (E′) and out-of-plane (A_1') vibrational peaks is observed for 1L MoS_2 on Au ($\Delta\omega \approx 21$ cm^{-1}) as compared to the case of 1L MoS_2 on Al_2O_3/Si ($\Delta\omega \approx 18$ cm^{-1}). Such a difference is due to significant red-shift of the E′ peak (mostly associated to the strain) and to a slight blue-shift of the A_1' peak (mostly related to the doping) for 1L MoS_2 membrane on gold. This is a typically observed behavior originating from the strong S–Au interaction, although slightly different $\Delta\omega$ values ($\Delta\omega \approx 20$ cm^{-1}) have been reported in other literature reports, probably due a to different quality of the MoS_2/Au interface.[31,32]

Interestingly, the E′ peak red-shift is further increased and the A_1' peak blue-shift is slightly reduced after ALD of the uniform Al_2O_3 film on the gold-supported membrane. On the other

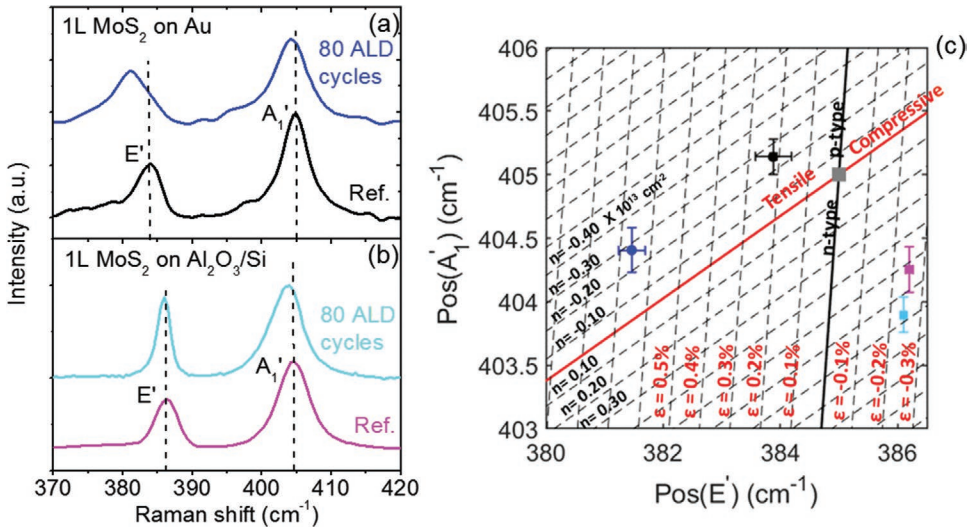

Figure 7. Representative Raman spectra collected on a) 1L MoS_2 on Au and b) 1L MoS_2 on Al_2O_3/Si before (reference) and after 80 Al_2O_3 ALD cycles. c) Correlative plot of the A_1' versus E′ peak frequencies of the Raman spectra acquired on the 1L MoS_2 on Au before (black circle) and after (blue circle) ALD deposition and for 1L MoS_2 on Al_2O_3/Si before (magenta square) and after (cyan square) ALD deposition, allowing to evaluate the type and average values of strain and doping of 1L MoS_2 membrane.

© 2021 The Authors. Advanced Materials Interfaces published by Wiley-VCH GmbH

hand, only a slight red-shift of the A_1' peak was observed after 80 ALD cycles on the Al_2O_3-supported 1L MoS_2, probably due to the inhomogeneous Al_2O_3 coverage (as shown in Figure 2a). In order to achieve a quantification of the strain, ε (%), and doping, n (cm^{-2}), for the 1L MoS_2 membranes on the two different substrates before and after the ALD process, a correlative analysis of the A_1' versus E′ peak frequencies has been carried out in Figure 7c, according to the procedure recently discussed in ref. [34]. The red and black lines in Figure 7c represent the theoretical behavior of the peaks' frequencies for 1L MoS_2 subjected only to a biaxial strain (tensile or compressive) or to doping (n-type or p-type), respectively. The crossing point (grey square) of these lines corresponds to literature values of the E′ and A_1' positions for a free-standing 1L MoS_2, taken as the best approximation for ideally unstrained and undoped MoS_2. The spacing of the dashed lines parallel to the ideal strain and doping lines is associated with carrier density changes of 0.1×10^{13} cm^{-2} and strain changes of 0.1%, respectively. The black point is the average value of the A_1' versus E′ frequencies from several (>20) Raman spectra measured on the reference 1L MoS_2/Au sample, whereas the error bars are the standard deviations from this statistical analysis. The magenta point is the average value obtained from Raman analyses on several points of the reference 1L MoS_2/Al_2O_3 sample. For this sample, the A_1' frequency exhibits a significant dispersion (indicated by the error bar), whereas the small E′ frequency dispersion is within the data point. According to the graphical analysis in Figure 7c, the reference 1L MoS_2/Au sample is characterized by an average tensile strain of $\varepsilon \approx 0.21\%$ and p-type doping of $n \approx -0.25 \times 10^{13}$ cm^{-2}, whereas an opposite compressive strain $\varepsilon \approx -0.25\%$ and n-type doping $n \approx 0.5 \times 10^{13}$ cm^{-2} are observed for 1L MoS_2 transferred onto the Al_2O_3/Si substrate. Such n-type behavior is consistent with the unintentional doping type commonly reported for exfoliated or CVD-grown MoS_2, which has been associated to the presence of defects (e.g., sulfur vacancies) or to other impurities in the MoS_2 lattice.[36,37] In the case of 1L MoS_2 on Au, a strong electron transfer to the substrate is guessed, which overcompensates the native n-type doping, resulting in a net p-type behavior.[34,38] This is consistent with several literature reports showing a transition from n- to p-type doping for MoS_2 layers functionalized with an $AuCl_3$ solution,[39] single Au atoms,[40] Au thin films,[41] as well as for MoS_2 deposited by gold nanoparticles-assisted CVD.[42]

The tensile strain for 1L MoS_2 on Au can be ascribed to the lattice mismatch between MoS_2 and the Au surface, mostly exposing (111) orientation.[43,44] According to recent literature reports, tensile strain of 1L MoS_2 is responsible of an enhanced reactivity on the basal plane, specifically at sulfur (S) vacancy sites.[45] Hence, the observed tensile strain of 1L MoS_2 exfoliated on Au substrates, combined with the presence of a very high density of native S vacancies in the material,[46] can also contribute to the enhanced Al_2O_3 nucleation during the early stages of thermal ALD. Furthermore, recent investigations of the vibrational properties for MoS_2/Au samples with variable MoS_2 thickness showed a significantly reduced effect of the MoS_2/Au interaction on 2L MoS_2 as compared to 1L samples.[38] These results would contribute to further explain the lower reactivity of 2L MoS_2/Au during the early stage of Al_2O_3 growth, as observed in Figure 6c,d.

Noteworthy, the blue point in Figure 7c obtained from Raman analyses after 80 ALD cycles on 1L MoS_2/Au indicates a further increase of the tensile strain ($\varepsilon \approx 0.65\%$), as compared to the original value of 0.21%, which can be associated to the formation of a compact Al_2O_3 film on top of MoS_2. On the other hand, no significant changes with respect to the original p-type doping value were observed after the ALD growth, confirming that the doping status of the film is strongly dominated by the strong Au–1L MoS_2 interaction. Finally, the data-point for the 1L MoS_2/Al_2O_3 sample after the 80 ALD cycles indicates no significant changes in the tensile strain, consistently with the highly inhomogeneous Al_2O_3 coverage, and an increase of the n-type doping to $n \approx 0.6 \times 10^{13}$ cm^{-2}. This latter can be ascribed to positively charged defects[47] at the interface between the poor quality Al_2O_3 film and 1L MoS_2.

Raman analyses clearly show very different strain and doping properties of 1L MoS_2 residing on the Au and Al_2O_3/Si substrates, which finally result in the growth of different quality Al_2O_3 films after ALD deposition.

In **Figure 8**, micro-PL spectra acquired on the two reference 1L MoS_2 samples and after 80 cycles ALD growth are also reported, to further elucidate the impact of the substrate and of the deposition process on the optical emission properties of the direct bandgap 1L MoS_2 membrane.

A prominent emission peak located at 1.84 eV can be observed for 1L MoS_2 supported by Al_2O_3/Si, whereas a significant reduction of the PL intensity accompanied by the red-shift of the main peak position at 1.79 eV is found for the reference sample on Au. A similar quenching of the PL intensity has been reported for 1L MoS_2 exfoliated on Au[34,48] and for MoS_2 functionalized with Au nanoparticles.[41] This behavior can be explained in terms of a preferential transfer of photoexcited charges from MoS_2 to Au. In addition, the tensile strain of 1L MoS_2 in contact with Au can also play a role in the reduction of the PL yield.[49] After 80 ALD cycles, only a small reduction of the PL intensity was observed for the 1L MoS_2/Al_2O_3 sample, which can be explained by the highly inhomogeneous Al_2O_3 coverage and by the small interaction of MoS_2 with the dielectric substrate. On the other hand, further quenching of the PL intensity was found in the case of 1L MoS_2/Au sample covered by the ≈3.6 nm uniform Al_2O_3 film. This observation can be consistent with the increase of the tensile strain observed by Raman analyses and with the

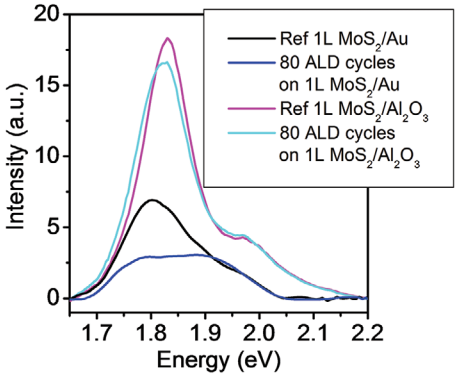

Figure 8. Micro-PL spectra acquired on 1L MoS_2/Al_2O_3 and on 1L MoS_2/Au samples before (ref. spectra) and after 80 Al_2O_3 ALD cycles.

© 2021 The Authors. Advanced Materials Interfaces published by Wiley-VCH GmbH

increase of the interaction with the Au substrate due to the material added on top of MoS_2.

3. Conclusion

In conclusion, we have demonstrated the direct thermal ALD growth at 250 °C of highly homogeneous and ultrathin (≈3.6 nm) Al_2O_3 films with excellent insulating properties onto a 1L MoS_2 membrane exfoliated on gold. Differently from the case of 1L MoS_2 supported by a common insulating substrate (Al_2O_3/Si), an enhanced nucleation of the high-*k* films was observed on the 1L MoS_2/Au system since the early stages of the ALD process, with the Al_2O_3 surface coverage increasing from ≈50% (after only 10 ALD cycles) to >90% (after 40 cycles). The coverage percentage was found to be significantly reduced in the case of 2L MoS_2/Au, indicating a crucial role of the S–Au interaction at the interface in the observed phenomena. Raman spectroscopy and PL analyses provided an insight about the role played by the tensile strain and p-type doping of 1L MoS_2 induced by the gold substrate on the enhanced high-*k* nucleation on MoS_2 surface.

The demonstrated high-quality ALD growth of high-*k* dielectrics on large-area 1L MoS_2 produced by the Au-assisted exfoliation can find important device applications, including the fabrication of FETs or the passivation of non-volatile switching memory devices based on Au/1L MoS_2/Au junctions. The development of an optimized transfer of the Al_2O_3/1L MoS_2 stack from Au to insulating or semiconductor substrates will represent a key enabling step for some of these technologies.

4. Experimental Section

The gold substrate used for MoS_2 mechanical exfoliation was prepared by sequentially depositing a 10 nm Ni adhesion layer and a 15 nm Au film with DC magnetron sputtering on top of a SiO_2/Si sample. MoS_2 exfoliation was performed by pressing a bulk molybdenite (2H-MoS_2) stamp on the surface of a freshly prepared Au/Ni/SiO_2 sample, in order to avoid the adsorption of contaminants (e.g., adventitious carbon) on Au surface, which would reduce the 1L MoS_2 exfoliation yield.[48] This process results in a large area mostly composed by 1L MoS_2 with some 2L regions identified by optical contrast, AFM, and Raman spectroscopy.

The Al_2O_3/Si substrate used for transferring the Au-exfoliated MoS_2 was prepared by DC-pulsed RF reactive sputtering of 100 nm Al_2O_3 on a Si wafer. The transfer procedure of the large-areas MoS_2 membranes from gold to this insulating substrate is discussed in details in ref. [34].

Thermal ALD of Al_2O_3 thin films on MoS_2 was carried out in a PE-ALD LL SENTECH Instruments GmbH reactor, using TMA and H_2O as the aluminum precursor and coreactant, respectively. All depositions were carried out at a temperature of 250 °C and with a pressure of 10 Pa. Initially, a process consisting of 80 ALD cycles was simultaneously carried out on both 1L MoS_2/Au and 1L MoS_2/Al_2O_3/Si systems, to compare the Al_2O_3 coverage uniformity. After observing the beneficial effect of the Au substrate on the uniformity of the Al_2O_3 growth on 1L MoS_2, the nucleation and growth mechanisms on the 1L MoS_2/Au were investigated in more details, by performing shorter ALD processes (10 and 40 deposition cycles). To assess the reproducibility of the results, the ALD growth experiments were performed on several (>10) sets of MoS_2/Au and MoS_2/Al_2O_3/Si samples prepared during different runs.

The surface roughness, coverage fraction, and thickness of the deposited Al_2O_3 on MoS_2 were evaluated by tapping mode AFM, morphology, and phase, using a DI3100 equipment by Bruker with Nanoscope V electronics. Sharp silicon tips with a curvature radius of 5 nm were used for these measurements. Furthermore, the electrical insulating properties of the very thin Al_2O_3 films deposited on 1L MoS_2/Au were evaluated by C-AFM analyses[50] using the TUNA module and Pt-coated silicon tips.

Micro-Raman spectroscopy and micro-PL measurements of MoS_2 on the different substrates before/after the ALD growth of Al_2O_3 were carried out using a Horiba HR-Evolution micro-Raman system with a confocal microscope (100× objective) and a laser excitation wavelength of 532 nm.

Acknowledgements

The authors acknowledge S. Di Franco (CNR-IMM) for the expert assistance in the sample preparation, and P. Fiorenza and G. Greco (CNR-IMM) for useful discussions. This paper was supported, in part, by the Italian Ministry for University and Research (MUR) in the framework of the FlagERA-JTC 2019 project "ETMOS". E.S. acknowledges the PON project EleGaNTe (ARS01_01007) funded by MUR for financial support. Part of the experiments was carried out using the facilities of the Italian Infrastructure Beyond Nano.

Open Access Funding provided by Consiglio Nazionale delle Ricerche within the CRUI-CARE Agreement.

Conflict of Interest

The authors declare no conflict of interest.

Data Availability Statement

The data that support the findings of this study are available from the corresponding author upon reasonable request.

Keywords

atomic force microscopy, atomic layer deposition, conductive atomic force microscopy, MoS_2, photoluminescence, Raman spectroscopy

Received: July 1, 2021
Revised: September 9, 2021
Published online: October 11, 2021

[1] K. F. Mak, C. Lee, J. Hone, J. Shan, T. F. Heinz, *Phys. Rev. Lett.* **2010**, *105*, 136805.
[2] A. Splendiani, L. Sun, Y. Zhang, T. Li, J. Kim, C.-Y. Chim, G. Galli, F. Wang, *Nano Lett.* **2010**, *10*, 1271.
[3] Y. Y. Illarionov, T. Knobloch, M. Jech, M. Lanza, D. Akinwande, M. I. Vexler, T. Mueller, M. C. Lemme, G. Fiori, F. Schwierz, T. Grasser, *Nat. Commun.* **2020**, *11*, 3385.
[4] F. Giannazzo, *Nat. Electron.* **2019**, *2*, 54.
[5] F. Giannazzo, G. Greco, F. Roccaforte, S. S. Sonde, *Crystals* **2018**, *8*, 70.
[6] B. Radisavljevic, A. Radenovic, J. Brivio, V. Giacometti, A. Kis, *Nat. Nanotechnol.* **2011**, *6*, 147.
[7] H. Liu, P. D. Ye, *IEEE Electron Device Lett.* **2011**, *33*, 546.
[8] A. Pakalla, M. Putkonen, in *Handbook of Deposition Technologies for Films and Coatings*, 3rd Ed., (Ed: P. M. Martin), Elsevier, New York **2010**, pp. 364–391.
[9] H. Liu, K. Xu, X. Zhang, P. D. Ye, *Appl. Phys. Lett.* **2012**, *100*, 152115.

© 2021 The Authors. Advanced Materials Interfaces published by Wiley-VCH GmbH

[10] T. Park, H. Kim, M. Leem, W. Ahn, S. Choi, J. Kim, J. Uh, K. Kwon, S.-J. Jeong, S. Park, Y. Kim, H. Kim, *RSC Adv.* **2017**, *7*, 884.
[11] S. McDonnell, B. Brennan, A. Azcatl, N. Lu, H. Dong, C. Buie, J. Kim, C. L. Hinkle, M. J. Kim, R. M. Wallace, *ACS Nano* **2013**, *7*, 10354.
[12] T. Nam, S. Seo, H. Kim, *J. Vac. Sci. Technol., A* **2020**, *38*, 030803.
[13] R. H. J. Vervuurt, W. M. M. Kessels, A. A. Bol, *Adv. Mater. Interfaces* **2017**, *4*, 1700232.
[14] E. Schilirò, R. Lo Nigro, F. Roccaforte, F. Giannazzo, *C* **2019**, *5*, 53.
[15] F. Giannazzo, E. Schilirò, R. Lo Nigro, F. Roccaforte, R. Yakimova, *Appl. Sci.* **2020**, *10*, 2440.
[16] G. Fisichella, E. Schilirò, S. Di Franco, P. Fiorenza, R. Lo Nigro, F. Roccaforte, S. Ravesi, F. Giannazzo, *ACS Appl. Mater. Interfaces* **2017**, *9*, 7761.
[17] Y.-S. Lin, P.-H. Cheng, K.-W. Huang, H.-C. Lin, M.-J. Chen, *Appl. Surf. Sci.* **2018**, *443*, 421.
[18] A. Iraiwa, D. Matsumura, H. Kawarada, *J. Appl. Phys.* **2016**, *120*, 084504.
[19] L. Cheng, X. Qin, A. T. Lucero, A. Azcatl, J. Huang, R. M. Wallace, K. Cho, J. Kim, *ACS Appl. Mater. Interfaces* **2014**, *6*, 11834.
[20] J. Yang, S. Kim, W. Choi, S. H. Park, Y. Jung, M.-H. Cho, H. Kim, *ACS Appl. Mater. Interfaces* **2013**, *5*, 4739.
[21] B. Huang, M. Zheng, Y. Zhao, J. Wu, J. T. L. Thong, *ACS Appl. Mater. Interfaces* **2019**, *11*, 35438.
[22] K. M. Price, K. E. Schauble, F. A. McGuire, D. B. Farmer, A. D. Franklin, *ACS Appl. Mater. Interfaces* **2017**, *9*, 23072.
[23] K. M. Price, S. Najmaei, C. E. Ekuma, R. A. Burke, M. Dubey, A. D. Franklin, *ACS Appl. Nano Mater.* **2019**, *2*, 4085.
[24] C. Wirtz, T. Hallam, C. P. Cullen, N. C. Berner, M. O'Brien, M. Marcia, A. Hirsch, G. S. Duesberg, *Chem. Commun.* **2015**, *51*, 16553.
[25] H. Zhang, G. Arutchelvan, J. Meersschaut, A. Gaur, T. Conard, H. Bender, D. Lin, I. Asselberghs, M. Heyns, I. Radu, W. Vandervorst, A. Delabie, *Chem. Mater.* **2017**, *29*, 6772.
[26] B. Dlubak, P. R. Kidambi, R. S. Weatherup, S. Hofmann, J. Robertson, *Appl. Phys. Lett.* **2012**, *100*, 173113.
[27] E. Schilirò, R. Lo Nigro, F. Roccaforte, I. Deretzis, A. La Magna, A. Armano, S. Agnello, B. Pecz, I. G. Ivanov, R. Yakimova, F. Giannazzo, *Adv. Mater. Interfaces* **2019**, *6*, 1900097.
[28] A. J. Pollard, E. W. Perkins, N. A. Smith, A. Saywell, G. Goretzki, A. G. Phillips, S. P. Argent, H. Sachdev, F. Muller, S. Hufner, S. Gsell, M. Fischer, M. Schreck, J. Osterwalder, T. Greber, S. Berner, N. R. Champness, P. H. Beton, *Angew. Chem., Int. Ed.* **2010**, *49*, 1794.
[29] H. Zhang, J. Sun, T. Low, L. Zhang, Y. Pan, Q. Liu, J. Mao, H. Zhou, H. Guo, S. Du, F. Guinea, H.-J. Gao, *Phys. Rev. B* **2011**, *84*, 245436.
[30] E. Schilirò, R. Lo Nigro, S. E. Panasci, F. M. Gelardi, S. Agnello, R. Yakimova, F. Roccaforte, F. Giannazzo, *Carbon* **2020**, *169*, 172.
[31] S. R. Desai, S. R. Madhvapathy, M. Amani, D. Kiriya, M. Hettick, M. Tosun, Y. Zhou, M. Dubey, J. W. Ager, D. Chrzan, A. Javey, *Adv. Mater.* **2016**, *28*, 4053.
[32] Y. Huang, Y.-H. Pan, R. Yang, L.-H. Bao, L. Meng, H.-L. Luo, Y.-Q. Cai, G.-D. Liu, W.-J. Zhao, Z. Zhou, L.-M. Wu, Z.-L. Zhu, M. Huang, L.-W. Liu, L. Liu, P. Cheng, K.-H. Wu, S.-B. Tian, C.-Z. Gu, Y.-G. Shi, Y.-F. Guo, Z. G. Cheng, J.-P. Hu, L. Zhao, G.-H. Yang, E. Sutter, P. Sutter, Y.-L. Wang, W. Ji, X.-J. Zho, H.-J. Gao, *Nat. Commun.* **2020**, *11*, 2453.
[33] F. Liu, W. Wu, Y. Bai, S. H. Chae, Q. Li, J. Wang, J. Hone, X.-Y. Zhu, *Science* **2020**, *367*, 903.
[34] S. E. Panasci, E. Schilirò, G. Greco, M. Cannas, F. M. Gelardi, S. Agnello, F. Roccaforte, F. Giannazzo, *ACS Appl. Mater. Interfaces* **2021**, *13*, 31248.
[35] W. Li, J. Zhou, S. Cai, Z. Yu, J. Zhang, N. Fang, T. Li, Y. Wu, T. Chen, X. Xie, H. Ma, K. Yan, N. Dai, X. Wu, H. Zhao, Z. Wang, D. He, L. Pan, Y. Shi, P. Wang, W. Chen, K. Nagashio, X. Duan, X. Wang, *Nat. Electron.* **2019**, *2*, 563.
[36] F. Giannazzo, G. Fisichella, A. Piazza, S. Agnello, F. Roccaforte, *Phys. Rev. B* **2015**, *92*, 081307(R).
[37] F. Giannazzo, G. Fisichella, G. Greco, S. Di Franco, I. Deretzis, A. La Magna, C. Bongiorno, G. Nicotra, C. Spinella, M. Scopelliti, B. Pignataro, S. Agnello, F. Roccaforte, *ACS Appl. Mater. Interfaces* **2017**, *9*, 23164.
[38] S. E. Panasci, E. Schilirò, F. Migliore, M. Cannas, F. M. Gelardi, F. Roccaforte, F. Giannazzo, S. Agnello, *Appl. Phys. Lett.* **2021**, *119*, 093103.
[39] X. Liu, D. Qu, J. Ryu, F. Ahmed, Z. Yang, D. Lee, W. J. Yoo, *Adv. Mater.* **2016**, *28*, 2345.
[40] H. Liu, D. Grasseschi, A. Dodda, K. Fujisawa, D. Olson, E. Kahn, F. Zhang, T. Zhang, Y. Lei, R. B. N. Branco, A. L. Elıas, R. C. Silva, Y.-T. Yeh, C. M. Maroneze, L. Seixas, P. Hopkins, S. Das, C. J. S. de Matos, M. Terrones, *Sci. Adv.* **2021**, *6*, eabc9308.
[41] U. Bhanu, M. R. Islam, L. Tetard, S. I. Khondaker, *Sci. Rep.* **2015**, *4*, 5575.
[42] L. Seravalli, M. Bosi, P. Fiorenza, S. E. Panasci, D. Orsi, E. Rotunno, L. Cristofolini, F. Rossi, F. Giannazzo, F. Fabbri, *Nanoscale Adv.* **2021**, *3*, 4826.
[43] C. Gong, C. Huang, J. Miller, L. Cheng, Y. Hao, D. Cobden, J. Kim, R. S. Ruoff, R. M. Wallace, K. Cho, X. Xu, Y. J. Chabal, *ACS Nano* **2013**, *7*, 11350.
[44] A. Bruix, J. A. Miwa, N. Hauptmann, D. Wegner, S. Ulstrup, S. S. Grønborg, C. E. Sanders, M. Dendzik, A. G. Cabo, M. Bianchi, J. V. Lauritsen, A. A. Khajetoorians, B. Hammer, P. Hofmann, *Phys. Rev. B* **2016**, *93*, 165422.
[45] H. Li, C. Tsai, A. L. Koh, L. Cai, A. W. Contryman, A. H. Fragapane, J. Zhao, H. S. Han, H. C. Manoharan, F. Abild-Pedersen, J. K. Nørskov, X. Zheng, *Nat. Mater.* **2016**, *15*, 48.
[46] P. Vancsó, G. Z. Magda, J. Peto, J.-Y. Noh, Y.-S. Kim, C. Hwang, L. P. Biró, L. Tapasztó, *Sci. Rep.* **2016**, *6*, 29726.
[47] E. Schilirò, P. Fiorenza, C. Bongiorno, C. Spinella, S. Di Franco, G. Greco, R. Lo Nigro, F. Roccaforte, *AIP Adv.* **2020**, *10*, 125017.
[48] M. Velický, G. E. Donnelly, W. R. Hendren, S. McFarland, D. Scullion, W. J. I. De Benedetti, G. C. Correa, Y. Han, A. J. Wain, M. A. Hines, D. A. Muller, K. S. Novoselov, H. D. Abruña, R. M. Bowman, E. J. G. Santos, F. Huang, *ACS Nano* **2018**, *2*, 10463.
[49] D. Lloyd, X. Liu, J. W. Christopher, L. Cantley, A. Wadehra, B. L. Kim, B. B. Goldberg, A. K. Swan, J. S. Bunch, *Nano Lett.* **2016**, *16*, 5836.
[50] F. Giannazzo, E. Schilirò, G. Greco, F. Roccaforte, *Nanomaterials* **2020**, *10*, 803.

© 2021 The Authors. Advanced Materials Interfaces published by Wiley-VCH GmbH